applied sciences

MDPI

Article

An Energy-Efficient Optimization Method for High-Speed Rail Communication Systems Assisted by Intelligent Reflecting Surfaces (IRS)

Cuiran Li *, Yongjie Lu, Jianli Xie and Zepeng Zhang

School of Electronics and Information Engineering, Lanzhou Jiaotong University, Lanzhou 730070, China; 11210718@stu.lzjtu.edu.cn (Y.L.); xiejl@mail.lzjtu.cn (J.X.); 13220079@stu.lzjtu.edu.cn (Z.Z.)
* Correspondence: licr@mail.lzjtu.cn

Abstract: This paper proposes an intelligent reflecting surface (IRS)-assisted energy efficiency optimization algorithm to address the problem of energy efficiency (EE) degradation in high-speed rail communication systems caused by line-of-sight link blockages between base stations and trains. The joint optimization of base station beamforming and IRS phase shifts is formulated as a variable-coupled energy efficiency maximization problem, subject to the base station's transmission power and the IRS unit's modulus constraints. This is known to be an NP-hard problem, making it challenging to obtain the global optimal solution. To tackle the issue of optimization variable coupling, an alternating optimization is employed to decompose the original problem into two sub-problems: base station beamforming and IRS phase-shift optimization. The Dinkelbach method is utilized to convert the fractional objective function into a difference form; then, the successive convex approximation (SCA) algorithm is applied to transform non-convex constraints into convex ones, which are solved using CVX. The Riemann conjugate gradient (RCG) algorithm can effectively solve the difficult unit module constraint. Finally, an alternating iterative strategy is employed to converge to a suboptimal solution. Our simulation results demonstrate that the proposed algorithm significantly enhances system efficiency with low computational complexity. Specifically, when the number of IRS reflecting elements is 64, the system's EE is improved by approximately 12.41%, 35.26%, and 37.96% compared to the semi-definite relaxation algorithm, the random phase shift approach, and no IRS scheme, respectively.

Keywords: IRS; high-speed rail communication; energy efficiency; beamforming; alternating optimization

check for updates

Citation: Li, C.; Lu, Y.; Xie, J.; Zhang, Z. An Energy-Efficient Optimization Method for High-Speed Rail Communication Systems Assisted by Intelligent Reflecting Surfaces (IRS). *Appl. Sci.* **2023**, *13*, 9401. https://doi.org/10.3390/app13169401

Academic Editor: Christos Bouras

Received: 25 July 2023
Revised: 13 August 2023
Accepted: 16 August 2023
Published: 18 August 2023

Copyright: © 2023 by the authors. Licensee MDPI, Basel, Switzerland. This article is an open access article distributed under the terms and conditions of the Creative Commons Attribution (CC BY) license (https://creativecommons.org/licenses/by/4.0/).

1. Introduction

With the integration and advancement of various communication technologies, high-speed trains (HSTs) are evolving from being information-centric to intelligent systems [1]. HSTs have become the preferred mode of transportation for many due to their speed, efficiency, safety, and quality of service [2]. The continuous increase in users and smart devices within the HST communication system has led to a significant rise in the data demand, resulting in higher energy consumption [3]. To meet the growing data requirements of users, a considerable number of active antennas and devices are added to the HST communication system, leading to higher hardware costs and energy consumption [4]. In the context of the next-generation wireless communication systems for HSTs, the surge in mobile devices and the accompanying data demand drive the need for designing more energy-efficient and eco-friendly communication systems, with energy efficiency being a crucial indicator of a green wireless network [5]. However, when the line-of-sight path between the base station (BS) and the train is blocked, it not only seriously affects the safety of train operation but also disrupts stable data connections for users, leading to a decrease in the energy efficiency of the HST communication system. These challenges prompt the exploration of intelligent techniques that can control the propagation environment while

minimizing energy consumption to assist the HST communication system. The intelligent reflecting surface (IRS) is considered a promising technology to enhance spectrum and energy efficiency in next-generation HST communication systems. Additionally, it effectively mitigates the rapid fluctuations in received signal strength caused by the Doppler effect [1].

IRS is considered a revolutionary technology for achieving green communications. Comprising a large number of low-cost passive reflecting elements, IRS forms a planar array that enhances the wireless network's performance by controlling the propagation environment [6]. First, IRS only reflects the received signals without amplification, eliminating the need for radio frequency (RF) chains, leading to lower energy consumption compared to traditional relays [7]. Second, it boasts the characteristics of cost effectiveness, simplicity, and easy deployment, as it can be shaped to fit various surfaces that are deployed alongside railway tracks, train windows, building facades, etc., providing a high degree of flexibility to the communication system [8]. Lastly, its integration does not require changes to be made to existing communication system standards.

The aforementioned advantages of IRS have motivated numerous researchers to extensively investigate the problem of energy efficiency maximization in IRS-assisted multiple-input single-output (MISO) communication systems [9]. In [10], the authors proposed a joint optimization method based on the Dinkelbach, fractional programming, and semidefinite relaxation (SDR) algorithms. The simulation results demonstrated that the IRS-assisted system achieved higher energy efficiency than the non-IRS-assisted system. The authors of [11] designed the transmit power allocation and IRS phase shifts, showing that the IRS-assisted system outperformed traditional relay systems in terms of energy efficiency. However, the failure to optimize BS beamforming in this study may lead to performance degradation. The authors of [12] developed an optimization framework that incorporates quadratic transformation, alternating optimization, and the weighted least square error. By using an alternating optimization strategy to decouple optimization variables and employing quadratic transformation and the weighted least square error, the problem was transformed into a convex problem to be solved. The simulation results verified the effectiveness of this optimization framework. The authors of [13] maximized the system energy efficiency by jointly optimizing BS beamforming and IRS phase shifts. The continuous convex approximation algorithm was used to optimize beamforming, while the SDR algorithm was used to optimize the IRS phase shifts. For the energy efficiency maximization problem addressed in [14], an effective method based on fractional programming and alternating optimization was proposed, leading to the attainment of a local optimal solution. The authors of [15,16] addressed the energy efficiency maximization problem, using the SDR algorithm to optimize IRS phase shifts. The distinction lies in the former study focusing on a small-cell scenario, while the latter studied a simultaneous wireless information and power transfer (SWIPT) scenario. To tackle energy efficiency optimization addressed in [17], the Dinkelbach algorithm was employed to handle the fractional function, followed by an efficient algorithm based on alternating optimization. Beamforming was solved using the SDR, MM, and Dinkelbach algorithms, while IRS phase shifts were solved using manifold optimization. The authors of [18] investigated resource allocation in IRS-assisted uplink systems, which is an NP-hard non-convex problem. A block-coordinate descent-based iterative method was proposed for solving the problem. The simulation results indicated that increasing the number of IRS elements could better improve the system's energy efficiency compared to increasing the number of BS antennas. For the BS beamforming subproblem addressed in [19], a maximum ratio transmission strategy was adopted, and, for the IRS phase-shift optimization subproblem, the optimal phase shift for the IRS was obtained using the sine–cosine algorithm. The authors of [20] employed the block-coordinate descent method to jointly optimize the BS beamforming vector, power, and phase shift matrix. The simulation results showed that the block-coordinate descent method exhibited rapid convergence, and the proposed scheme achieved a 70.7% gain in energy efficiency compared to the non-IRS scheme. Although the aforementioned works have significantly improved the energy efficiency of IRS-assisted communication systems,

they mainly rely on optimization methods such as the SDR algorithm and the penalty function, which have high computational complexity [21]. Moreover, these works overlook the impact of the Doppler effect on the system's energy efficiency, reducing the applicability of the algorithms to IRS-assisted HST communication scenarios.

For IRS-assisted HST communication systems, ref. [22] aims to address communication blockages, enhance spectrum efficiency, and reduce outage probability by utilizing statistical channel state information (CSI) to investigate the outage performance of the MIMO system. A closed-form expression for the outage probability is derived. Furthermore, under the constraint of transmit power, the joint design of transmit-and-receive beamforming and an IRS phase shift is conducted to minimize the outage probability. In [23], a deep reinforcement learning framework combining LSTM and DDPG is proposed to design the BS transmit beamforming and IRS phase shift for millimeter-wave HST networks, thereby improving the system's spectrum efficiency. In order to enhance the anti-interference capability of the high-speed train network, ref. [24] addresses the capacity maximization problem for an IRS-assisted high-speed train network in the presence of interference. An IRS phase-shift optimization scheme based on deep deterministic policy gradients (DDPG) is proposed. Additionally, the issue of external interference threatening train safety is considered, and the interference suppression problem is transformed into a maximum-received signal-to-noise ratio problem, which is solved using the SDR algorithm [25]. However, the high complexity of the SDR algorithm hinders its large-scale application in HST communication systems. In [26], an optimization algorithm for joint transmit-and-receive beamforming and IRS phase shifts is proposed to enhance the capacity of IRS-assisted millimeter-wave HST communication systems. The numerical results demonstrate that deploying IRS in the system increases the system's capacity while reducing its power consumption. The existing literature on IRS-assisted HST communication systems primarily focuses on the performance analysis related to the outage probability, spectrum efficiency, and channel capacity, with relatively limited research into optimizing systems' energy efficiency.

Based on the aforementioned research findings, this paper considers the influence of the Doppler effect on channel modeling in the IRS-assisted HST communication scenario, taking into account the complexity reduction of algorithms and the improvement of system energy efficiency. The main contributions of this paper are as follows:

1. Addressing the problem of decreased system energy efficiency due to line-of-sight blockages between the BS and mobile relay in the HST communication system. We analyze the Doppler spreading of non-line-of-sight (NLOS) components in the direct BS–mobile relay link and the Doppler frequency shift in the IRS–mobile relay reflected link under the movement of a high-speed train. An IRS-assisted HST communication system model is established, considering the BS transmit power constraint and the IRS unit modulus constraint, formulating a joint optimization problem of BS transmit beamforming and the IRS phase shift for energy efficiency maximization. This problem involves multi-variable-coupled non-convex fractional programming, which is challenging to solve directly.
2. To tackle this NP-hard problem, a solution approach is proposed. First, to address the issue of optimizing variable coupling, an alternating optimization strategy is employed to decouple the variables, dividing the original problem into two sub-problems: BS transmit beamforming and IRS phase-shift optimization. For the BS transmit beamforming sub-problem, the Dinkelbach method is utilized to convert the fractional objective function into a difference form, and then the successive convex approximation (SCA) algorithm is used to transform non-convex constraints into convex ones, which are solved using CVX. For the IRS phase-shift sub-problem, the Riemannian conjugate gradient (RCG) algorithm is used for optimization. Finally, an alternating iterative process is conducted to converge to a suboptimal solution.
3. Through simulations conducted under different system parameters, such as the number of IRS elements and the BS transmit power, the results demonstrate the effectiveness of the proposed algorithm in enhancing the energy efficiency of IRS-assisted HST

communication systems compared to baseline algorithms. It is further confirmed that increasing the number of IRS elements is more cost effective, in terms of improving HST communication systems' energy efficiency, than increasing the number of BS antennas, thus proving the necessity of employing IRS in HST communication systems.

The rest of this article is organized as follows. In Section 2, we present the IRS-assisted HST communication system model. The energy efficiency optimization problem is formulated based on the proposed model. AO-EE algorithms for the optimization design are presented in Section 3. In Section 4, we provide numerical simulations and analysis. In Section 5, the conclusions of this paper and future research directions are presented.

2. System Modeling and Optimization Problems

2.1. IRS-Assisted HST Communication Models

This paper considers an IRS-assisted HST communication system model, as shown in Figure 1, where a mobile relay (MR) located on top of the train is utilized to receive signals to avoid train penetration losses [27]. The system consists of an M-antenna base station (BS), an IRS with N reflecting elements, where the distance between the reflecting elements $d_z = d_y = \lambda/2$,λ is the wavelength [22], and a single-antenna MR. The IRS is deployed along the railway on the side of the BS. It is assumed that the line-of-sight (LOS) component between the BS and MR is obstructed by obstacles, and the IRS is used to establish an auxiliary link to enhance the received signal strength. Furthermore, it is assumed that both the BS and IRS have perfect channel state information (CSI) [28].

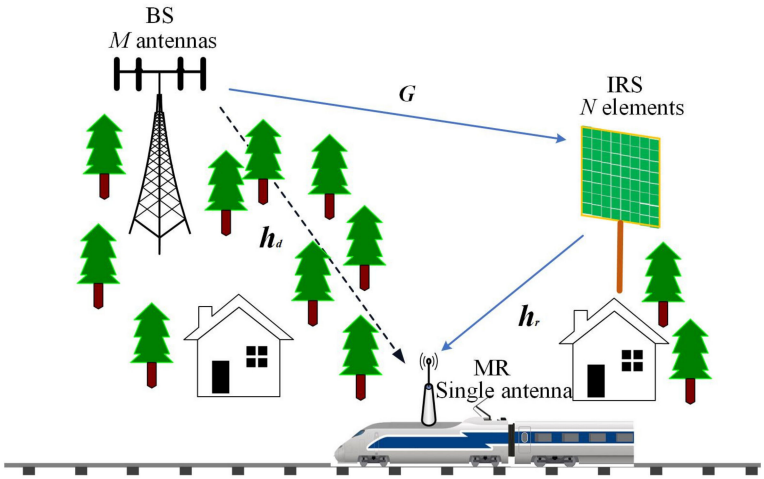


Figure 1. IRS-assisted HST communication system model.

Considering multiple equally sized time slots denoted as t within a time period T, each slot maintains constant signal characteristics. This assumption holds when the train's velocity remains constant [29]. Let $x(t) \in \mathbb{C}$ represent the information symbols transmitted by the base station (BS) in time slot t, subject to constraints: $\mathbb{E}\{x(t)\} = 0$ and $\mathbb{E}\left\{x(t)x(t)^H\right\} = 1$. Moreover, $\boldsymbol{f}(t) \in \mathbb{C}^{M\times 1}$ denotes the BS's transmit beamforming vector in time slot t. Consequently, the received signal at the mobile relay (MR) in time slot t is given by:

$$y(t) = \left(\boldsymbol{h}_r^H(t)\boldsymbol{\Theta}(t)\boldsymbol{G}(t) + \boldsymbol{h}_d^H(t)\right)\boldsymbol{f}(t)x(t) + \boldsymbol{n}(t), \tag{1}$$

where $\boldsymbol{h}_d(t) \in \mathbb{C}^{M\times 1}$ represents the channel gain of the BS–MR link in time slot t, and $\boldsymbol{G}(t) \in \mathbb{C}^{N\times M}$ and $\boldsymbol{h}_r(t) \in \mathbb{C}^{N\times 1}$ represent the channel gains of the BS–IRS and IRS–MR reflection links in time slot t, respectively. $\boldsymbol{n}(t) \sim \mathcal{CN}(0, \sigma^2)$ is the additive white Gaussian noise with power σ^2. The reflection coefficient matrix of the IRS is denoted as $\boldsymbol{\Theta} = \mathrm{diag}\left\{\beta_1 e^{j\theta_1}, \cdots, \beta_n e^{j\theta_n}, \cdots, \beta_N e^{j\theta_N}\right\}$. Let $\boldsymbol{V} = [v_1, \cdots, v_n, \cdots, v_N]^H$, where $v_n = \beta_n e^{j\theta_n}$, j is imaginary units. $\beta_n \in [0, 1]$ and $\theta_n \in [0, 2\pi)$ represent the amplitude and

phase shift of the nth reflecting element of the IRS, typically set as $\beta_1 = \beta_2 = \cdots = \beta_N = 1$ and $|v_n| = 1$ [22], respectively. Due to significant path loss, multiple reflections from the IRS are neglected [28].

Therefore, the signal-to-noise ratio (SNR) of the MR's received signal in time slot t is:

$$\gamma(t) = \frac{\left|\left(\boldsymbol{h}_r^H(t)\boldsymbol{\Theta}(t)\boldsymbol{G}(t) + \boldsymbol{h}_d^H(t)\right)\boldsymbol{f}(t)\right|^2}{\sigma^2}, \tag{2}$$

where $|\cdot|$ indicates the absolute value of a complex number.

2.2. Channel Model

Blockages are widespread in the high-speed train communication environment, where random obstacles are distributed along the railway [30]. It is assumed that the direct link between the BS and MR is obstructed by obstacles such as trees, and only the non-line-of-sight (NLOS) component is available to transmit the signal to the MR. Therefore, the direct link is modeled as Rayleigh fading, with a Doppler power spectral density following the Jakes spectrum.

Assuming that both the BS and MR antennas adopt a uniform linear array (ULA) architecture, and the IRS antennas adopt a uniform planar array (UPA) architecture, the antenna response vectors at the BS and MR ends are given by [24]:

$$\boldsymbol{a}(\theta) = \left[1, e^{j\frac{2\pi}{\lambda}d\sin\theta}, \cdots, e^{j\frac{2\pi}{\lambda}d(N-1)\sin\theta}\right]^{\mathrm{T}}, \tag{3}$$

The IRS consists of N reflecting elements, thus assuming $\sqrt{N}$ elements in both the horizontal and vertical directions. The steering vectors of the IRS along the y-axis and z-axis are given by [31]

$$p_y(\varphi,\theta) = \left[1, e^{j2\pi\frac{d_y}{\lambda}\sin\theta\cos\varphi}, \cdots, e^{j2\pi\frac{d_y}{\lambda}(\sqrt{N}-1)\sin\theta\cos\varphi}\right]^{\mathrm{T}}, \tag{4}$$

$$p_z(\theta) = \left[1, e^{j2\pi\frac{d_z}{\lambda}\cos\theta}, \cdots, e^{j2\pi\frac{d_z}{\lambda}(\sqrt{N}-1)\cos\theta}\right]^{\mathrm{T}}, \tag{5}$$

Since the BS and IRS locations have been deployed in advance and the BS–IRS is designated as line-of-sight transmission, the BS–IRS channel is modeled as [22]:

$$\boldsymbol{G} = \alpha p_y\left(\varphi_{IRS}^{AOA}, \theta_{IRS}^{AOA}\right) \otimes p_z\left(\theta_{IRS}^{AOA}\right) a^H\left(\theta_{BS}^{AOD}\right), \tag{6}$$

where $\otimes$ indicates the Kronecker product, α represents the complex channel gain of the BS-IRS link. $\varphi_{IRS}^{AOA} \in [0,\pi]$ and $\theta_{IRS}^{AOA} \in [0,\pi]$ represent the azimuth and pitch angles of the signal arriving at the IRS, respectively. $\theta_{BS}^{AOD} \in [0,\pi]$ represents the departure angle of the BS transmitter signal.

For IRS–MR links, channel $\boldsymbol{h}_{r,n}$ under the nth time slot is assumed to obey Rice fading [22]:

$$\boldsymbol{h}_{r,n} = \sqrt{\frac{k}{k+1}}\overline{\boldsymbol{h}}_{r,n} + \sqrt{\frac{1}{k+1}}\widetilde{\boldsymbol{h}}_{r,n}, \tag{7}$$

where k is the Rician K factor, $\widetilde{\boldsymbol{h}}_{r,n}$ is the NLOS component in the nth time slot of the IRS-MR link, which follows a Rayleigh distribution with a Jakes spectrum of power expansion, and $\overline{\boldsymbol{h}}_{r,n}$ is the LOS component affected by the Doppler frequency shift. Therefore, $\overline{\boldsymbol{h}}_{r,n}$ is:

$$\overline{\boldsymbol{h}}_{r,n} = \beta p_y\left(\varphi_{IRS}^{AOD}, \theta_{IRS}^{AOD}\right) \otimes p_z\left(\theta_{IRS}^{AOD}\right) e^{j2\pi f_d n T_c}, \tag{8}$$

where β denotes the complex gain of the IRS–MR link. $\varphi_{IRS}^{AOD} \in [0, \pi]$ and $\theta_{IRS}^{AOD} \in [0, \pi]$ denote the azimuth and pitch angles of the reflected signal leaving the IRS, respectively. f_d denotes the Doppler shift.

The following discussion focuses on one time slot only, and t is omitted from the following discussion. The achievable rate R at MR is:

$$R = \log_2\left(1 + \frac{\left|\left(\boldsymbol{h}_r^H \boldsymbol{\Theta} \boldsymbol{G} + \boldsymbol{h}_d^H\right)\boldsymbol{f}\right|^2}{\sigma^2}\right), \tag{9}$$

The total power consumption of the IRS-assisted HST communication system includes the BS transmit signal power, the circuit consumption of the BS and MR, and the power consumption of the IRS reflection unit. Thus, the total power consumption of the system is [32]:

$$P_{all} = \frac{1}{\xi}\|\boldsymbol{f}\|^2 + P_{BS} + P_{IRS} + P_{MR}, \tag{10}$$

where ξ is the power amplification efficiency of the BS. Let $\xi = 1$ [32]. P_{BS} indicates the circuit power consumption of the BS. $P_{IRS} = NP_R$, where P_R denotes the power consumption generated by each reflective element of the IRS. P_{MR} is the relay forwarding power. Note that (10) can only be used under two assumptions: (1) the transmit amplifier operates in its linear region, and (2) the last three power consumptions do not depend on the rate of the communication link [11].

Energy efficiency is defined as the data rate per unit of energy. This is the ratio of the data rate to the total power consumption [32]:

$$EE = \frac{R}{P_{all}}, \tag{11}$$

Energy efficiency (EE) is measured in bit/Joule.

2.3. Modeling Optimization Problems

Based on the communication system model shown in Figure 1, this section maximizes the system energy efficiency under the BS transmit power and IRS phase constraints by jointly designing the BS transmit beamforming and the IRS phase shift. The IRS-assisted energy efficiency optimization problem for HST communication systems is modeled:

$$\begin{aligned} \mathrm{P1}: \max_{\boldsymbol{f},\boldsymbol{\Theta}} \frac{R}{P_{all}} &= \frac{\log\left(1+\frac{\left|\left(\boldsymbol{h}_r^H \boldsymbol{\Theta} \boldsymbol{G} + \boldsymbol{h}_d^H\right)\boldsymbol{f}\right|^2}{\sigma^2}\right)}{\frac{1}{\xi}\|\boldsymbol{f}\|^2 + P_{BS} + NP_R + P_{MR}} \\ \text{s.t. } \mathrm{C1}&: \|\boldsymbol{f}\|^2 \le P_{\max} \\ \mathrm{C2}&: |v_n| = 1 \quad \forall n = 1, \cdots, \mathrm{N} \end{aligned} \tag{12}$$

where $\|\cdot\|$ denotes the Euclidean Paradigm operator. In the context of the optimization problem P1, where $P_{\max}$ represents the BS transmit power, C1 represents the maximum BS transmit power constraint, and C2 represents the IRS unit modulus constraint. Solving the problem becomes challenging due to the strong coupling between variables $\boldsymbol{f}$ and $\boldsymbol{\Theta}$, while also satisfying the constraint C2 on the IRS phase shifts. It is a continuous optimization problem [33]. To address this issue, we adopt an alternating optimization strategy to decouple the variables. Specifically, we decompose problem P1 into two sub-problems: the BS transmit beamforming sub-problem and the IRS phase-shift optimization sub-problem. By iteratively solving these two sub-problems in an alternating manner, we achieve convergence.

3. Optimization Problem Solving

Due to the fractional structure of the objective function in problem P1 and the strong coupling between the optimization variables, directly obtaining a solution is challenging. To address this issue, we adopt an alternating optimization strategy to decouple P1 into two sub-problems: (1) fixing the IRS phase-shift matrix and optimizing the BS transmit beamforming, and (2) fixing the BS transmit beamforming and optimizing the IRS phase-shift matrix. For sub-problem (1), we utilize the Dinkelbach-SCA algorithm. Specifically, since the objective function is in a fractional form, the Dinkelbach algorithm is employed to transform it into a parameter subtraction form. Considering the presence of non-convex constraints, the SCA algorithm is used to convert the non-convex problem into a solvable convex optimization problem. The CVX toolbox [34] is then utilized to obtain the optimal BS transmit beamforming. For sub-problem (2), the Riemannian Conjugate Gradient (RCG) algorithm is employed to optimize the IRS phase-shift matrix. The optimization process is then iteratively alternated between BS transmit beamforming and the IRS phase shift until convergence.

3.1. Optimizing BS Transmit Beamforming for a Given IRS Phase Shift

For a given IRS phase shift $\boldsymbol{\Theta}$, problem P1 can be rewritten as:

$$\begin{aligned} \text{P2}: \max_{\boldsymbol{f}} \ & \frac{R}{P_{all}} \\ \text{s.t. C1}: & \|\boldsymbol{f}\|^2 \le P_{\max} \end{aligned} \tag{13}$$

Since the objective function of P2 is a fractional function, it is first transformed into an easily handled phase-reduction form [35].

Theorem 1. *Let $R(\boldsymbol{f}^*) > 0, P_{all}(\boldsymbol{f}^*) > 0$ be the optimal achievable rate and the minimum total power consumption, respectively, for problem P2. Let $\mathcal{F}$ be the feasible solution set of problem P2. Assume that the energy efficiency of the system is maximized when the BS transmit beamforming is $\boldsymbol{f}^*$, such that:*

$$\lambda^* = \frac{R(\boldsymbol{f}^*)}{P_{all}(\boldsymbol{f}^*)} = \max_{\boldsymbol{f}\in\mathcal{F}} \left\{ \frac{R(\boldsymbol{f})}{P_{all}(\boldsymbol{f})} \right\} \tag{14}$$

If and only if $R(\boldsymbol{f}^*), P_{all}(\boldsymbol{f}^*), \lambda^*$ satisfy the following condition:

$$\max_{\boldsymbol{f}\in\mathcal{F}} \{R(\boldsymbol{f}) - \lambda^* P_{all}(\boldsymbol{f})\} = R(\boldsymbol{f}^*) - \lambda^* P_{all}(\boldsymbol{f}^*) = 0 \tag{15}$$

Thus, the parametric programming with parameter λ is defined as [35]:

$$\max_{\boldsymbol{f},\lambda} \{R(\boldsymbol{f}) - \lambda P_{all}(\boldsymbol{f})\} \tag{16}$$

Proof of Theorem 1. See Appendix A. □

According to Theorem 1, by introducing the energy efficiency factor λ, P2 is equivalently expressed as:

$$\begin{aligned} \text{P2}-1: \max_{\boldsymbol{f}} \ & [R(\boldsymbol{f}) - \lambda\, P_{all}(\boldsymbol{f})] \\ = \max_{\boldsymbol{f}} & \log_2\left(1 + \frac{\left|\left(\boldsymbol{h}_r^H \boldsymbol{\Theta} \boldsymbol{G} + \boldsymbol{h}_d^H\right)\boldsymbol{f}\right|^2}{\sigma^2}\right) \\ & -\lambda \left(\frac{1}{\xi}\|\boldsymbol{f}\|^2 + P_{BS} + NP_R + P_{MR}\right) \\ \text{s.t. C1}: & \|\boldsymbol{f}\|^2 \le P_{\max} \end{aligned} \tag{17}$$

λ is updated with $\lambda_{\mathrm{i}} = R(\boldsymbol{f}_{\mathrm{i}})/P_{all}(\boldsymbol{f}_i)$ from λ_0, until $|\lambda_i - \lambda_{i-1}| \le \varepsilon$ is satisfied. ε is the convergence threshold.

Given that λ_i solves problem P2-1, maximizing a function is equivalent to maximizing the lower bound of that function. Since the logarithmic function is increasing monotonically, this is equivalent to finding a lower bound on $\left|\left(\boldsymbol{h}_r^H\boldsymbol{\Theta}\boldsymbol{G}+\boldsymbol{h}_d^H\right)\boldsymbol{f}\right|^2$. Let $\boldsymbol{a}=\boldsymbol{h}_r^H\boldsymbol{\Theta}\boldsymbol{G}+\boldsymbol{h}_d^H$, $\boldsymbol{A}=\boldsymbol{a}^H\boldsymbol{a}$. We obtain:

$$\left|\left(\boldsymbol{h}_r^H\boldsymbol{\Theta}\boldsymbol{G}+\boldsymbol{h}_d^H\right)\boldsymbol{f}\right|^2=|\boldsymbol{a}\,\boldsymbol{f}|^2=\left|\boldsymbol{f}^H\boldsymbol{a}^H\boldsymbol{a}\,\boldsymbol{f}\right|=\left|\boldsymbol{f}^H\boldsymbol{A}\boldsymbol{f}\right|, \tag{18}$$

Let $r=1/\sigma^2$. The lower bound of $\boldsymbol{f}^H\boldsymbol{A}\boldsymbol{f}$ is s. Then, the problem P2-1 is equivalently expressed as:

$$\begin{aligned}\mathrm{P2-2}:\max_{\boldsymbol{f},s}\ &\log_2(1+rs)-\lambda_i\left(\tfrac{1}{\xi}\|\boldsymbol{f}\|^2+P_{BS}+NP_R+P_{MR}\right)\\ \text{s.t. C1}:\ &\|\boldsymbol{f}\|^2\le P_{\max}\\ \text{C3}:\ &\boldsymbol{f}^H\boldsymbol{A}\,\boldsymbol{f}\ge s\end{aligned} \tag{19}$$

Since C3 is a nonconvex constraint, the convex function $\boldsymbol{f}^H\boldsymbol{A}\boldsymbol{f}$ is approximated by a first-order Taylor approximation, and the SCA algorithm is used to perform a first-order Taylor expansion at the feasible point $\hat{\boldsymbol{f}}$:

$$\boldsymbol{f}^H\boldsymbol{A}\,\boldsymbol{f}\ge 2\mathrm{Re}\left\{\hat{\boldsymbol{f}}^H\boldsymbol{A}\,\boldsymbol{f}\right\}-\hat{\boldsymbol{f}}^H\boldsymbol{A}\,\hat{\boldsymbol{f}}, \tag{20}$$

The nonconvex constraint can be replaced by a tighter convex constraint, given by the following equation:

$$2\mathrm{Re}\left\{\hat{\boldsymbol{f}}^H\boldsymbol{A}\boldsymbol{f}\right\}-\hat{\boldsymbol{f}}^H\boldsymbol{A}\hat{\boldsymbol{f}}\ge s, \tag{21}$$

By replacing constraint C3 with (19), problem P2-2 is rewritten as:

$$\begin{aligned}\mathrm{P2-3}:\max_{\boldsymbol{f},s}\ &\log_2(1+rs)-\lambda_i\left(\tfrac{1}{\xi}\|\boldsymbol{f}\|^2+P_{BS}+NP_R+P_{MR}\right)\\ \text{s.t. C1}:\ &\|\boldsymbol{f}\|^2\le P_{\max}\\ \text{C4}:\ &2\mathrm{Re}\left\{\hat{\boldsymbol{f}}^H\boldsymbol{A}\boldsymbol{f}\right\}-\hat{\boldsymbol{f}}^H\boldsymbol{A}\hat{\boldsymbol{f}}\ge s\end{aligned} \tag{22}$$

P2–3 are convex problems that can be solved by the standard solver of CVX [34], Problems P2–3 are solved by repeatedly updating the vector that assigns the optimal result of the previous solution, which gives the BS transmit beamforming.

The Dinkelbach-SCA algorithm optimizes the BS transmit beamforming, as shown in Algorithm 1.

Algorithm 1. Dinkelbach-SCA algorithm for problem P2.

1: **Initialization:** $\hat{\boldsymbol{f}},\boldsymbol{f}_0,\lambda_0,i=j=0,\varepsilon=10^{-3}$;
2: **repeat**
3: Calculate $\boldsymbol{a}=\boldsymbol{h}_r^H\boldsymbol{\Theta}\boldsymbol{G}+\boldsymbol{h}_d^H$ and $\boldsymbol{A}=\boldsymbol{a}^H\boldsymbol{a}$;
4: **repeat**
5: Calculate $2\mathrm{Re}\left\{\hat{\boldsymbol{f}}^H\boldsymbol{A}\boldsymbol{f}\right\}-\hat{\boldsymbol{f}}^H\boldsymbol{A}\hat{\boldsymbol{f}}$ according to (21);
6: Update $\hat{\boldsymbol{f}}=\boldsymbol{f}_j$, Solving P2-3 with CVX;
7: $j=j+1$;
8: **until** the objective value of (P2-2) with the obtained $\boldsymbol{f}_j$ reaches convergence;
9: $i=i+1$;
10: Update $\lambda_{\mathrm{i}}=R(\boldsymbol{f}_{\mathrm{i}})/P_{all}(\boldsymbol{f}_i)$;
11: **Until** $|\lambda_i-\lambda_{i-1}|\le\varepsilon$.

3.2. Optimizing the IRS Phase Shift for a Given BS Transmit Beamforming

Given the BS transmit beamforming, problem P1 is reformulated as:

$$\begin{aligned} \text{P3}: \max_{\boldsymbol{\Theta}} \ & \log_2\left(1+\frac{\left|\left(\boldsymbol{h}_r^H\boldsymbol{\Theta}\boldsymbol{G}+\boldsymbol{h}_d^H\right)\boldsymbol{f}\right|^2}{\sigma^2}\right) \\ \text{s.t. C2}: & |v_n|=1 \quad \forall \text{n}=1,\cdots,\text{N} \end{aligned} \tag{23}$$

Problem P3 can be rewritten as:

$$\begin{aligned} \text{P3}-1: \max_{\boldsymbol{\Theta}} \ & \left|\left(\boldsymbol{h}_r^H\boldsymbol{\Theta}\boldsymbol{G}+\boldsymbol{h}_d^H\right)\boldsymbol{f}\right|^2 \\ \text{s.t. C2}: & |v_n|=1 \quad \forall \text{n}=1,\cdots,\text{N} \end{aligned} \tag{24}$$

Using the properties of diagonal matrices, we have $\boldsymbol{h}_r^H\boldsymbol{\Theta}\boldsymbol{G}=\boldsymbol{V}^H\text{diag}\left(\boldsymbol{h}_r^H\right)\boldsymbol{G}$.

$$\left|\left(\boldsymbol{h}_r^H\boldsymbol{\Theta}\boldsymbol{G}+\boldsymbol{h}_d^H\right)\boldsymbol{f}\right|^2=\left|\left(\boldsymbol{V}^{\text{H}}\text{diag}\left(\boldsymbol{h}_r^H\right)\boldsymbol{G}+\boldsymbol{h}_d^H\right)\boldsymbol{f}\right|^2, \tag{25}$$

Let $\boldsymbol{F}=\boldsymbol{f}\boldsymbol{f}^H$. Issue P3-1 is reissued as:

$$\begin{aligned} \text{P3}-2: \min_{\boldsymbol{V}} & \boldsymbol{f}_C(\boldsymbol{V})=-\boldsymbol{V}^H\mathbf{Y}\boldsymbol{V}-\boldsymbol{V}^H\mathbf{b}-\mathbf{b}^H\boldsymbol{V} \\ \text{s.t.} & |v_n|=1 \quad \forall \text{n}=1,\cdots,\text{N}, \end{aligned} \tag{26}$$

where $\mathbf{Y}=\text{diag}\left(\boldsymbol{h}_r^H\right)\boldsymbol{G}\boldsymbol{F}\boldsymbol{G}^H\text{diag}(\boldsymbol{h}_r)$, $\mathbf{b}=\text{diag}\left(\boldsymbol{h}_r^H\right)\boldsymbol{G}\boldsymbol{F}\boldsymbol{h}_d$.

Problem P3-2 is solved using the Riemann Conjugate Gradient (RCG) algorithm [36]. The main idea of the RCG algorithm is to generalize the conjugate gradient method from Euclidean space to manifold space, and its main task is to compute the Euclidean gradient. The RCG algorithm has three key steps in each iteration:

1. Compute the Riemannian gradient: the Riemannian gradient is a tangent vector (direction) of the fastest-growing objective function, and the Riemannian gradient is the Euclidean orthogonal projection of the Euclidean gradient $\nabla\boldsymbol{f}_C$ onto the complex circle:

$$\text{grad}\boldsymbol{f}_C=\nabla\boldsymbol{f}_C-\text{Re}\{\nabla\boldsymbol{f}_C\circ\boldsymbol{V}^*\}\circ\boldsymbol{V}, \tag{27}$$

where the Euclidean gradient is:

$$\nabla\boldsymbol{f}_C=2(\mathbf{Y}\boldsymbol{V}+\mathbf{b}), \tag{28}$$

2. Search direction: using the obtained Riemannian gradient, the optimization of Euclidean spaces is extended to manifold spaces. The search directions η_i and η_{i+1} are located in different tangent spaces. Thus, mapping the tangent vector η_i from $T_{V_i}\mathcal{M}$ to $T_{V_{i+1}}\mathcal{M}$ requires a transmission operation $\mathcal{I}_{V_i\to V_{i+1}}(\eta_i)$, i.e., the tangent vector conjugate to $\text{grad}\boldsymbol{f}_C$ can be found as the search direction

$$\begin{aligned} \nabla\boldsymbol{f}_C=2(\mathbf{Y}\boldsymbol{V}+\mathbf{b})\mathcal{I}_{V_i\to V_{i+1}}(\eta_i): T_{V_i}\mathcal{M}\mapsto T_{V_{i+1}}\mathcal{M}: \\ \eta_i\mapsto\eta_i-\text{Re}\left\{\eta_i\circ\boldsymbol{V}_{i+1}^*\right\}\circ\boldsymbol{V}_{i+1} \end{aligned} \tag{29}$$

The search directions are updated for:

$$\eta_{i+1}=-\text{grad}\boldsymbol{f}_C+\tau_i\cdot\mathcal{I}_{\boldsymbol{V}_i\to\boldsymbol{V}_{i+1}}(\eta_i), \tag{30}$$

where τ_i is the Polak–Ribiere parameter.

3. Retraction: After determining the search direction η_i, it is necessary to determine the Armijo step size β_i, and the resulting point $\beta_i\cdot\eta_i$ may leave the stream. The resulting

point may leave the manifold. Therefore, it is necessary to map the tangent vector from the tangent space back to the manifold itself:

$$\beta_i \eta_i \mapsto \frac{(\boldsymbol{V}_i + \beta_i \eta_i)_n}{|(\boldsymbol{V}_i + \beta_i \eta_i)_n|}, \tag{31}$$

where $(\boldsymbol{V}_i + \beta_i \eta_i)_n$ denotes item n of $\boldsymbol{V}_{i+1} \alpha_i \nabla \boldsymbol{f}_C$.

The RCG algorithm optimizes the IRS phase shift, as shown in Algorithm 2.

Algorithm 2. RCG Algorithm for optimizing the reflection coefficients.

1: **Initialization:** $\boldsymbol{V}_0$,$\eta_i = -\text{grad}\boldsymbol{f}_C$, $i = 0$,$\varepsilon = 10^{-3}$;
2: **repeat**
3: Choose the Armijo backtracking line search step size α_i;
4: Find the next point $\boldsymbol{V}_{i+1}$ using retraction in (31);
5: Calculate the Euclidean gradient $\nabla \boldsymbol{f}_C$ according to (28);
6: Calculate the Riemannian gradient $\text{grad}\boldsymbol{f}_C$ according to (27);
7: Calculate the transport $\mathcal{I}_{\boldsymbol{V}_i \to \boldsymbol{V}_{i+1}}(\eta_i)$ according to (29);
8: Calculate the conjugate direction η_i according to (30);
9: $i = i + 1$;
10: **Until** $\|\text{grad}\boldsymbol{f}_C\|_2 \leq \varepsilon$.
11: **Output:** $\boldsymbol{V}^* = \boldsymbol{V}_i$.

3.3. Convergence and Algorithm Complexity Analysis

The proposed alternating optimization-based energy efficiency (AO-EE) optimization algorithm is shown in Algorithm 3.

Algorithm 3 AO-EE Algorithm for problem P1.

1: **Initialization:** $\boldsymbol{f}_0$, $\boldsymbol{V}_0$ is randomly generated, $i = 0$, $\varepsilon = 10^{-3}$;
2: **repeat**
3: Calculate $\boldsymbol{V}_{i+1}$ based on Algorithm 1 with fixed $\boldsymbol{f}_i$;
4: Calculate $\boldsymbol{f}_{i+1}$ based on Algorithm 1 with fixed $\boldsymbol{V}_i$;
5: **Until** The increase of the objective value of the problem P1 is below the threshold ε.

The convergence performance of AO-EE needs to be proven, as follows.

We define $\boldsymbol{f}_i$, $\boldsymbol{V}_i$ as the i-th iteration solution of the problems (P2), (P3). The objective function is denoted by $EE(\boldsymbol{f}_i, \boldsymbol{V}_i)$. In step 3 of Algorithm 3, the BS transmit beamforming vector can be obtained for a given $\boldsymbol{V}_i$. Hence, we have:

$$EE(\boldsymbol{f}_i, \boldsymbol{V}_i) \leq EE(\boldsymbol{f}_{i+1}, \boldsymbol{V}_i) \tag{32}$$

In step 4 of Algorithm 3, we can obtain an IRS phase shift when $\boldsymbol{f}_i$ is given. We have:

$$EE(\boldsymbol{f}_{i+1}, \boldsymbol{V}_i) \leq EE(\boldsymbol{f}_{i+1}, \boldsymbol{V}_{i+1}) \tag{33}$$

Thus, we obtain:

$$EE(\boldsymbol{f}_i, \boldsymbol{V}_i) \leq EE(\boldsymbol{f}_{i+1}, \boldsymbol{V}_{i+1}) \tag{34}$$

Therefore, $EE(\boldsymbol{f}_i, \boldsymbol{V}_i)$ is non-decreasing over the iterations in the AO-EE, and $EE(\boldsymbol{f}_i, \boldsymbol{V}_i)$ has the upper bound due to the transmit power constraint. Thus, the AO-EE algorithm is guaranteed to converge.

To validate the effectiveness of the proposed AO-EE algorithm, we compare it with five benchmark algorithms, as follows:

1. No-IRS scheme: this scheme does not consider IRS-related channels and only optimizes the BS transmit beamforming using the Dinkelbach-SCA algorithm, denoted as "NO-IRS".

2. Random phase-shift scheme: in this scheme, the phase of each reflecting element is uniformly and independently generated from $[0, 2\pi]$ randomly, and the BS transmit beamforming is optimized using the Dinkelbach-SCA algorithm, denoted as the "random phase".
3. SDR scheme: the IRS phase-shift optimization is conducted using the SDR algorithm [28], while the BS transmit beamforming is optimized using the Dinkelbach-SCA algorithm, denoted as "baseline scheme1".
4. Phase alignment scheme: the IRS phase-shift optimization is performed using phase alignment [28], and the BS transmit beamforming is optimized using the Dinkelbach-SCA algorithm, denoted as "Baseline scheme2".
5. SDR-SDR scheme: Both the BS transmit beamforming and IRS phase shift are optimized using the SDR algorithm [37], denoted as "Baseline scheme3".

The complexity analysis of the AO-EE algorithm is as follows: to solve the BS transmit beamforming, the Dinkelbach and SCA algorithms are used, and the complexity of solving problem P2-3 is $\mathcal{O}(M^3)$ [38]. The IRS phase shift is optimized using the Riemannian Conjugate Gradient (RCG) algorithm, where the main complexity lies in calculating the Euclidean gradient, which is $\mathcal{O}(N^2)$. The backtracking step also requires an iterative search for τ_2, but its complexity can be neglected when N is large. Therefore, the complexity of the RCG algorithm is $\mathcal{O}(N^2)$ [39]. Let the iterations of the Dinkelbach algorithm, SCA algorithm, and alternating optimization be L_1, L_2, and I_{iter}, respectively. The overall complexity of the AO-EE algorithm is $\mathcal{O}\left(I_{iter}\left(L_1L_2M^3 + N^2\right)\log_2\left(\frac{1}{\varepsilon}\right)\right)$, where ε is the convergence threshold.

The computational complexities of the proposed algorithm and three benchmark IRS optimization algorithms are shown in Table 1. In addition, we compared the running time of the proposed algorithm with those of Baseline Scheme 1 for a single iteration, and recorded the running time for five iterations, as shown in Table 2. It can be observed that the proposed AO-EE algorithm has relatively low complexity.

Table 1. Algorithmic complexity.

Beamforming Design Method	Algorithmic Complexity
AO-EE	$\mathcal{O}\left(I_{iter}\left(L_1L_2M^3 + N^2\right)\log_2\left(\frac{1}{\varepsilon}\right)\right)$
Baseline Scheme 1	$\mathcal{O}\left(I_{iter}\left(L_1L_2M^3 + N^{3.5}\right)\log_2\left(\frac{1}{\varepsilon}\right)\right)$
Baseline Scheme 2	$\mathcal{O}\left(I_{iter}\left(L_1L_2M^3 + N\right)\log_2\left(\frac{1}{\varepsilon}\right)\right)$
Baseline Scheme 3	$\mathcal{O}\left(I_{iter}\left(M^{3.5} + N^{3.5}\right)\log_2\left(\frac{1}{\varepsilon}\right)\right)$

Table 2. Running time of each iteration.

Beamforming Design Method	Running Time When N = 64 (Unit: s)				
AO-EE	7.4414	6.8477	7.6923	7.0585	6.9890
Baseline Scheme 1	437.2063	428.4659	439.2299	424.3579	439.9219

4. Simulation Results and Analysis

In this section, the energy efficiency performance of the proposed AO-EE algorithm is simulated, considering the IRS-assisted HST communication system's downlink. In the 3D Cartesian coordinate system, the coordinates of BS, IRS, and MR are set to (0 m, 0 m, 10 m), (0 m, 150 m, 2.5 m), and (10 m, 140 m, 2.5 m), respectively; the carrier frequency $f_C = 5$ GHz, the system bandwidth B = 100 KHz, and the train speed v = 70 m/s. The BS transmit power Pmax = 42 dBm, the Rician K-factor is set to 10, the noise power $\sigma^2 = -110$ dBm and $d = \lambda/2$. λ is the wavelength [22], the BS static power consumption $P_{BS} = 40$ dBm, and the MR power consumption $P_{MR} = 30$ dBm [40]. The power consumption of the IRS unit $P_R = 10$ dBm [11], and the maximum Doppler shift $f_m = vf_c/c \approx 1167$ Hz, where c is the

speed of light. The time slot length is set to the correlation time $T_c = 0.432/f_m \approx 0.3$ ms. Due to the random nature of a single experiment, all numerical simulation results are averaged over 500 independent channel realizations. The simulation is performed using the MATLAB simulation platform. The running environment is Intel(R) Core (TM) i7-13700F (2.1 GHz), NVIDIA RTX4070Ti.

For large-scale fading, a distance-based path loss model is used [25]:

$$L(d) = C_0 \left(\frac{d}{d_0} \right)^{-\alpha} \tag{35}$$

where $C_0 = -30$ dB, denotes the path loss at the reference distance $d_0 = 1$ m, d denotes the link distance, α denotes the path loss exponent, and the path loss coefficients for BS-MR, BS-IRS, and IRS-MR are $\alpha_{BM} = 3.5$, $\alpha_{BI} = 2$, and $\alpha_{IM} = 2.5$, respectively [25].

Figure 2 illustrates the relationship between the number of IRS reflecting elements (N) and the system energy efficiency for different algorithms when $M = 32$ and $P_{\max} = 42$ dBm. It can be observed that, in the absence of IRS (the NO-IRS case), increasing the number of IRS reflecting elements has no impact on the system's energy efficiency, resulting in a linear relationship. As the number of IRS reflecting elements increases, the system's energy efficiency for the other five IRS algorithms (Random Phase, Baseline Scheme 1, Baseline Scheme 2, and Baseline Scheme 3) shows varying degrees of improvement. This improvement is attributed to the gain achieved from both the BS transmit beamforming and the aperture gain provided by IRS, whereas the NO-IRS algorithm only benefits from the gain in the BS transmit beamforming. All four IRS optimization algorithms outperform the Random Phase algorithm, to a significant degree. This demonstrates the necessity of optimizing the IRS phase shift, as, under random phase shifts, the reflected signals may not be properly directed towards the MR, resulting in a substantial reduction in the gains offered by IRS. Furthermore, a similarity is observed in the system performance of the Baseline Scheme 1, Baseline Scheme 2, and Baseline Scheme 3 algorithms. However, when $N = 64$, the proposed AO-EE algorithm surpasses them, achieving approximately 12.41% higher system energy efficiency. Comparing the proposed AO-EE algorithm with the NO-IRS and Random Phase schemes, the system energy efficiency is improved by approximately 35.26% and 37.96%, respectively. Hence, the proposed AO-EE algorithm strikes a favorable balance between computational complexity and system energy efficiency.

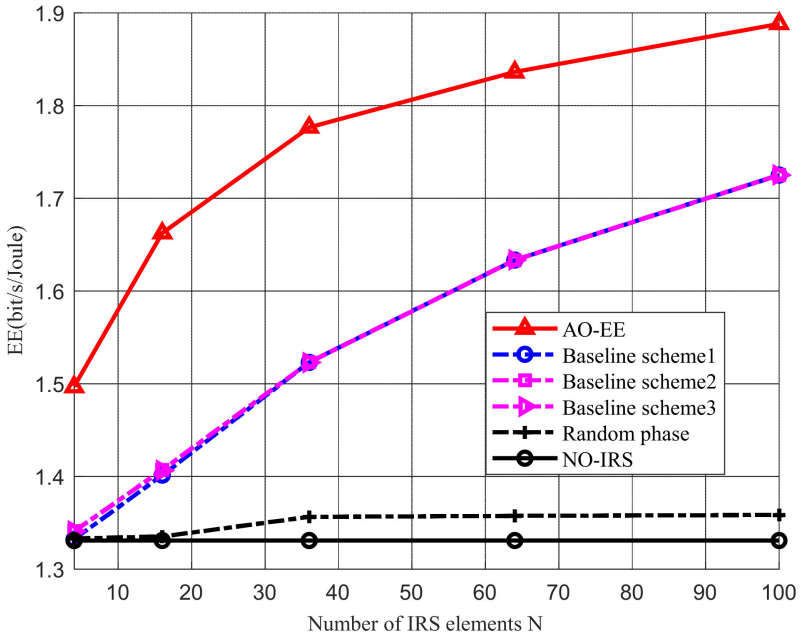


Figure 2. EE versus the number of IRS elements.

Figure 3 presents the relationship between the BS transmit power and the system energy efficiency for different algorithms with $M = 32$ and $N = 64$. It can be observed that, as the BS transmit power increases, the system energy efficiency gradually improves. This improvement arises because the BS transmit power affects the range of values for BS transmit beamforming. However, due to saturation effects, when the BS transmit power reaches a certain threshold, further increasing the power will lead to a plateau in the system energy efficiency. Under the same BS transmit power, the proposed AO-EE algorithm outperforms the baseline schemes in terms of achieving higher system energy efficiency. Furthermore, the performances of the Random Phase and NO-IRS schemes show few differences from each other. Therefore, for IRS-assisted HST communication systems, optimizing the IRS phase shift is essential to enhancing the system energy efficiency. In conclusion, Figure 3 demonstrates that increasing the BS transmit power can lead to improved system energy efficiency. The proposed AO-EE algorithm consistently achieves better performance than the baseline schemes. Additionally, optimizing the IRS phase shift is crucial for enhancing the energy efficiency of IRS-assisted HST communication systems.

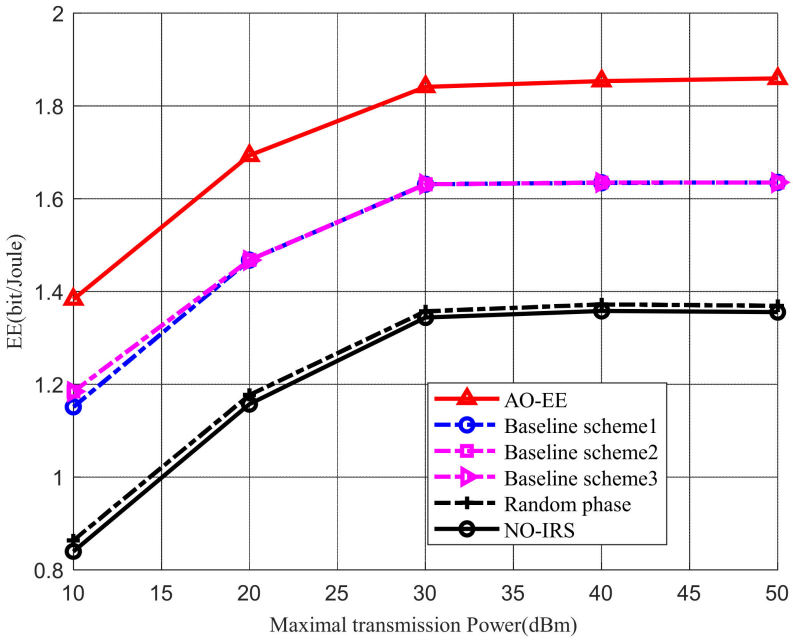


Figure 3. EE versus maximum transmit power $P_{\max}$.

Figure 4 illustrates the relationship between the number of BS antennas (M) and the system energy efficiency for different algorithms, with $N = 64$ and $P_{\max} = 42$ dBm. It can be observed that, as the number of BS antennas increases, the system energy efficiency gradually improves. This improvement is attributed to the higher array gain achieved when there are more BS antennas, leading to increased system energy efficiency. With the same number of BS antennas, the proposed AO-EE algorithm consistently outperforms the baseline schemes in terms of achieving higher system energy efficiency. Furthermore, the energy efficiency of the IRS-assisted system surpasses that of the NO-IRS scheme, validating the effectiveness of deploying IRS in HST communication systems. In conclusion, Figure 4 demonstrates that increasing the number of BS antennas results in improved system energy efficiency, owing to the higher diversity gain obtained with more antennas. The proposed AO-EE algorithm consistently outperforms the baseline schemes, and the deployment of IRS in HST communication systems proves to be effective in enhancing energy efficiency.

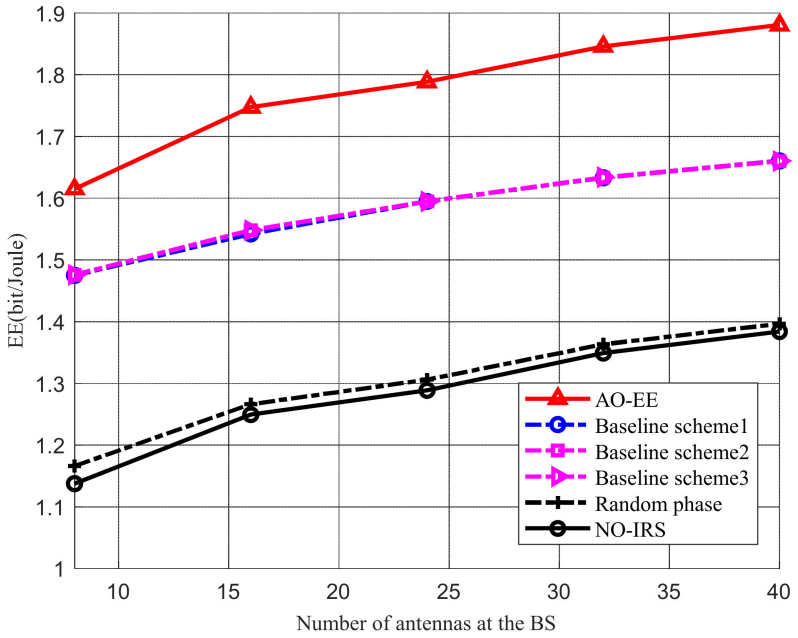


Figure 4. EE versus the number of BS antennas.

Figure 5 illustrates the variation in system energy efficiency with the number of IRS reflecting elements for $M = 32$ using the proposed AO-EE algorithm at different transmit powers. It can be observed that the three curves exhibit the same trend: as the number of IRS elements increases, the system energy efficiency also improves for different BS transmit powers. Furthermore, when operating with the same number of IRS reflecting elements, the system energy efficiency increases with the growth of the transmit power. This is because a higher transmit power allows the BS to allocate more power for signal transmission to meet the power constraint, leading to an increase in system energy efficiency. However, as indicated in Figure 3, due to the saturation effect, the relationship between transmit power and system energy efficiency does not increase in a linear manner. Therefore, deploying IRS in HST communication systems requires a careful consideration of both the transmit power and the number of IRS elements to achieve optimal system performance.

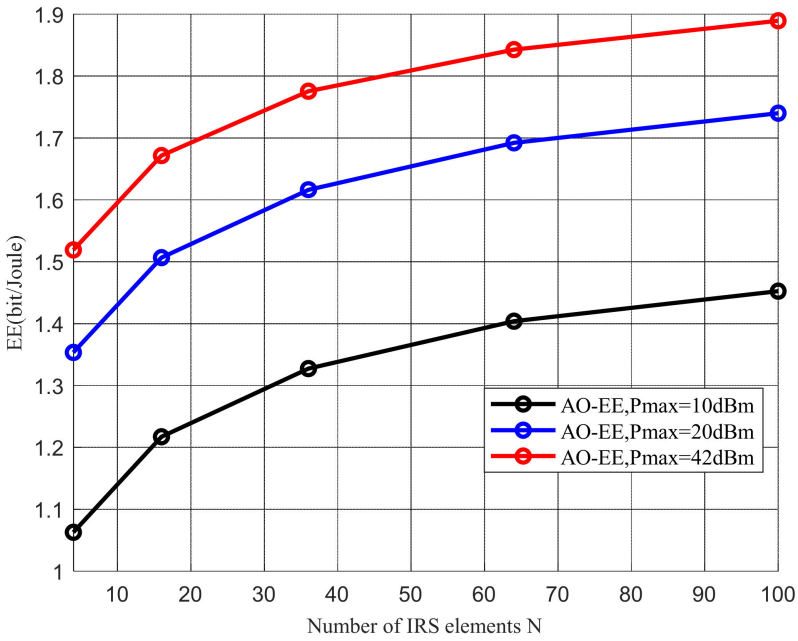


Figure 5. EE versus the number of IRS elements at different transmit powers.

Figure 6 illustrates the variation in the system energy efficiency with BS transmit power for $M = 32$ using the proposed AO-EE algorithm at different numbers of IRS reflecting elements. From Figure 6, it can be observed that, as the BS transmit power increases, the system energy efficiency initially improves and then reaches a plateau for different numbers of IRS reflecting elements. Furthermore, under the same BS transmit power, the system energy efficiency increases with the growth in the number of IRS reflecting elements. This is because a larger number of IRS elements can reflect more received signals from the BS, leading to an increase in system energy efficiency. In summary, the results in Figure 6 demonstrate that increasing the BS transmit power and the number of IRS reflecting elements can enhance the system energy efficiency in an IRS-assisted HST communication system.

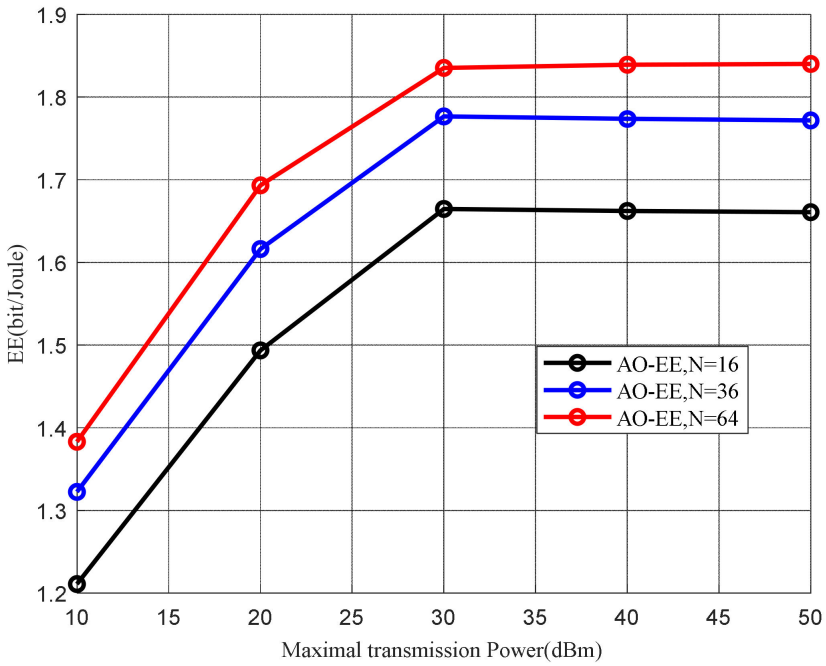


Figure 6. EE versus transmit power for different numbers of IRS elements.

Figure 7 illustrates the energy efficiency advantages of an IRS-assisted HST communication system over a traditional multi-antenna HST communication system. In the traditional HST communication system, increasing the number of BS antennas can improve the system's energy efficiency. In Figure 7, three scenarios are considered: 1. Setting the number of BS antennas to $M = 16$ and increasing the number of IRS reflecting elements; 2. Setting the number of IRS elements to $N = 16$ and increasing the number of BS antennas; 3. No IRS, and increasing the number of BS antennas. It can be observed that the system energy efficiency with IRS assistance is higher than that without IRS, indicating that increasing the number of IRS reflecting elements is more effective in improving system energy efficiency than increasing the number of BS transmit antennas. Therefore, IRS can economically and effectively enhance the system energy efficiency. Furthermore, the proposed AO-EE algorithm's system energy efficiency outperforms Baseline Scheme 1, proving the effectiveness of the proposed algorithm.

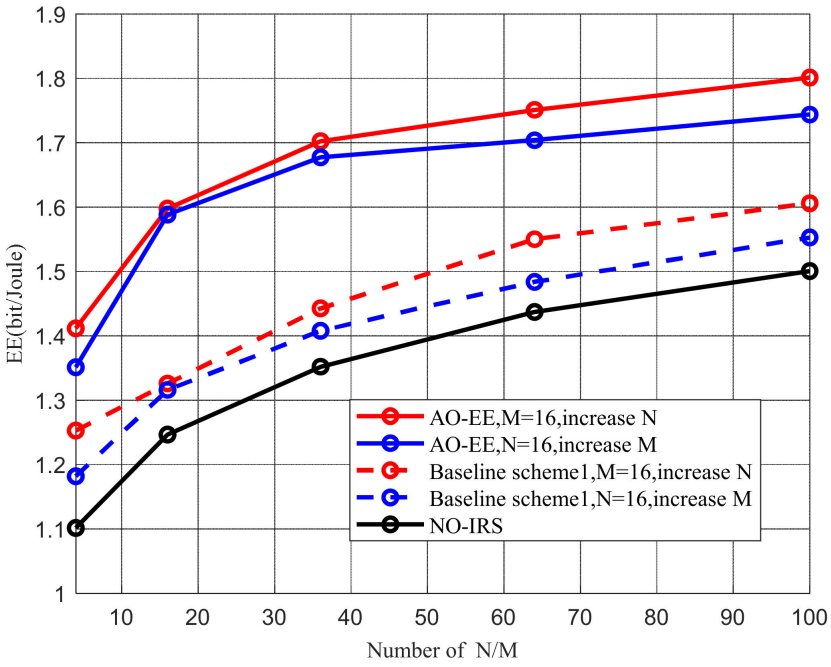


Figure 7. EE versus the number of N/M in different schemes.

5. Conclusions

In this study, we address the problem of maximizing energy efficiency in an IRS-assisted HST communication system by considering essential physical constraints. We formulate a multi-variable-coupled energy efficiency optimization problem and employ an alternating optimization strategy to decouple the variables. The Dinkelbach and SCA algorithms are utilized to convert the non-convex problem into convex ones to solve for BS transmit beamforming. The RCG algorithm is used to optimize the IRS phase shifts. The simulation results demonstrate that the IRS-assisted HST communication system indeed enhances system energy efficiency. Specifically, when the number of IRS reflecting elements is 64, the system EE is improved by approximately 12.41%, 35.26%, and 37.96% compared to the semi-definite relaxation algorithm, the random phase-shift approach, and the scheme with no IRS, respectively. Compared to traditional HST communication systems that increase energy efficiency by adding more BS antennas, increasing the number of IRS elements can economically and effectively boost the system energy efficiency, making the HST communication system greener and more energy-efficient.

In future research, considering the complexity of railway environments, we suggest investigating the use of advanced techniques such as deep reinforcement learning and other AI methods to optimize the energy efficiency of IRS-assisted HST communication systems. Given the difficulty of acquiring accurate information about the ideal CSI, future research should look towards investigating the performance of IRS-assisted HST communication systems in the presence of an imperfect CSI.

Author Contributions: Conceptualization, C.L., Y.L., J.X. and Z.Z.; methodology, C.L., Y.L., J.X. and Z.Z.; validation, C.L., Y.L., J.X. and Z.Z.; writing—original draft preparation, Y.L.; writing—review and editing, C.L. and J.X.; supervision, C.L. All authors have read and agreed to the published version of the manuscript.

Funding: This research was funded by the National Natural Science Foundation of China (62161016), the Science and Technology Plan of Gansu Province (20JR10RA273), and the Beijing Engineering Research Center of High-Speed Railway Broadband Mobile Communications (BHRC-2022-1), Beijing Jiaotong University.

Institutional Review Board Statement: Not applicable.

Informed Consent Statement: Not applicable.

Data Availability Statement: Not applicable.

Conflicts of Interest: The authors declare no conflict of interest. The funders had no role in the design of the study; in the collection, analyses, or interpretation of data; in the writing of the manuscript; or in the decision to publish the results.

Appendix A

Let f^* be the optimal solution of problem P2, where $\mathcal{F}$ is a feasible set for problem P2. For all $f \in \mathcal{F}$ values, we have:

$$\lambda^* = \frac{R(f^*)}{P_{all}(f^*)} \geq \frac{R(f)}{P_{all}(f)} \tag{A1}$$

Hence:

$$R(f) - \lambda^* P_{all}(f) \leq 0 \tag{A2}$$

$$R(f^*) - \lambda^* P_{all}(f^*) = 0 \tag{A3}$$

From the inequality in Equation (A2), we have $\max_f \{R(f) - \lambda^* P_{all}(f)\} = 0$. The maximum value is taken from (A3) when $f = f^*$. The sufficient condition has been proved.

Next, consider the proof of the necessary conditions. Let f^* be a solution of $\max_f \{R(f) - \lambda^* P_{all}(f)\} = 0$, Thus, we have $R(f^*) - \lambda^* P_{all}(f^*) = 0$. Then, for all $f \in \mathcal{F}$ values, we have:

$$R(f) - \lambda^* P_{all}(f) \leq 0 \tag{A4}$$

$$R(f^*) - \lambda^* P_{all}(f^*) = 0 \tag{A5}$$

From Equation (A4), we obtain $\lambda^* \geq R(f)/P_{all}(f)$ for all $f \in \mathcal{F}$ values, and λ^* is the maximum objective value of the problem P2. This completes the proof of Theorem 1.

References

1. Zhang, J.; Liu, H.; Wu, Q.; Jin, Y.; Chen, Y.; Ai, B.; Jin, S.; Cui, T.J. RIS-aided next-generation high-speed train communications: Challenges, solutions, and future directions. *IEEE Wirel. Commun.* **2021**, *28*, 145–151. [CrossRef]
2. Sharma, H.K.; Majumder, S.; Biswas, A.; Prentkovskis, O.; Kar, S.; Skačkauskas, P. A Study on Decision-Making of the Indian Railways Reservation System during COVID-19. *J. Adv. Transp.* **2022**, *2022*, 7685375. [CrossRef]
3. Hu, J.; Wang, X.; Xu, Y. Energy-efficient power optimization and transmission mode selection for distributed antenna system in HSR communications. In Proceedings of the 2019 IEEE 89th Vehicular Technology Conference (VTC2019-Spring), Kuala Lumpur, Malaysia, 28 April–1 May 2019; pp. 1–5.
4. Khan, R.; Kumar, P.; Jayakody, D.N.K.; Liyanage, M. A survey on security and privacy of 5G technologies: Potential solutions, recent advancements, and future directions. *IEEE Commun. Surv. Tutor.* **2019**, *22*, 196–248. [CrossRef]
5. Wu, Q.; Zhang, R. Towards smart and reconfigurable environment: Intelligent reflecting surface aided wireless network. *IEEE Commun. Mag.* **2019**, *58*, 106–112. [CrossRef]
6. Di Renzo, M.; Zappone, A.; Debbah, M.; Alouini, M.-S.; Yuen, C.; De Rosny, J.; Tretyakov, S. Smart radio environments empowered by reconfigurable intelligent surfaces: How it works, state of research, and the road ahead. *IEEE J. Sel. Areas Commun.* **2020**, *38*, 2450–2525. [CrossRef]
7. Wu, Q.; Zhang, R. Beamforming optimization for wireless network aided by intelligent reflecting surface with discrete phase shifts. *IEEE Trans. Commun.* **2019**, *68*, 1838–1851. [CrossRef]
8. Wu, Q.; Zhang, R. Joint active and passive beamforming optimization for intelligent reflecting surface assisted SWIPT under QoS constraints. *IEEE J. Sel. Areas Commun.* **2020**, *38*, 1735–1748. [CrossRef]
9. Zheng, B.; You, C.; Mei, W.; Zhang, R. A survey on channel estimation and practical passive beamforming design for intelligent reflecting surface aided wireless communications. *IEEE Commun. Surv. Tutor.* **2022**, *24*, 1035–1071. [CrossRef]
10. Quispe, J.J.; Maciel, T.F.; Silva, Y.C.; Klein, A. RIS-assisted beamforming for energy efficiency in multiuser downlink transmissions. In Proceedings of the 2022 IEEE Globecom Workshops (GC Wkshps), Rio de Janeiro, Brazil, 4–8 December 2022; pp. 1543–1548.
11. Huang, C.; Zappone, A.; Alexandropoulos, G.C.; Debbah, M.; Yuen, C. Reconfigurable intelligent surfaces for energy efficiency in wireless communication. *IEEE Trans. Wirel. Commun.* **2019**, *18*, 4157–4170. [CrossRef]
12. Zhang, M.; Tan, L.; Huang, K.; You, L. On the trade-off between energy efficiency and spectral efficiency in RIS-aided multi-user MISO downlink. *Electronics* **2021**, *10*, 1307. [CrossRef]

13. Fang, F.; Xu, Y.; Pham, Q.-V.; Ding, Z. Energy-efficient design of IRS-NOMA networks. *IEEE Trans. Veh. Technol.* **2020**, *69*, 14088–14092. [CrossRef]
14. Du, L.; Zhang, W.; Ma, J.; Tang, Y. Reconfigurable intelligent surfaces for energy efficiency in multicast transmissions. *IEEE Trans. Veh. Technol.* **2021**, *70*, 6266–6271. [CrossRef]
15. Wang, Q.; Zhou, F.; Hu, R.Q.; Qian, Y. Energy-efficient beamforming and cooperative jamming in IRS-assisted MISO networks. In Proceedings of the ICC 2020—2020 IEEE International Conference on Communications (ICC), Dublin, Ireland, 7–11 June 2020; pp. 1–7.
16. Liu, J.; Xiong, K.; Lu, Y.; Ng, D.W.K.; Zhong, Z.; Han, Z. Energy efficiency in secure IRS-aided SWIPT. *IEEE Wirel. Commun. Lett.* **2020**, *9*, 1884–1888. [CrossRef]
17. Zargari, S.; Khalili, A.; Zhang, R. Energy efficiency maximization via joint active and passive beamforming design for multiuser MISO IRS-aided SWIPT. *IEEE Wirel. Commun. Lett.* **2020**, *10*, 557–561. [CrossRef]
18. Zeng, M.; Bedeer, E.; Dobre, O.A.; Fortier, P.; Pham, Q.-V.; Hao, W. Energy-efficient resource allocation for IRS-assisted multi-antenna uplink systems. *IEEE Wirel. Commun. Lett.* **2021**, *10*, 1261–1265. [CrossRef]
19. Tan, F.; Xu, X.; Chen, H.; Li, S. Energy-efficient beamforming optimization for MISO communication based on reconfigurable intelligent surface. *Phys. Commun.* **2023**, *57*, 101996. [CrossRef]
20. Li, G.; Zeng, M.; Mishra, D.; Hao, L.; Ma, Z.; Dobre, O.A. Energy-efficient joint beamforming design for IRS-assisted MISO system. In Proceedings of the 2021 IEEE International Conference on Communications Workshops (ICC Workshops), Montreal, QC, Canada, 14–23 June 2021; pp. 1–6.
21. Li, Z.; Wang, S.; Lin, Q.; Li, Y.; Wen, M.; Wu, Y.-C.; Poor, H.V. Phase shift design in RIS empowered wireless networks: From optimization to AI-based methods. *Network* **2022**, *2*, 398–418. [CrossRef]
22. Gao, M.; Ai, B.; Niu, Y.; Han, Z.; Zhong, Z. IRS-assisted high-speed train communications: Outage probability minimization with statistical CSI. In Proceedings of the ICC 2021-IEEE International Conference on Communications, Montreal, QC, Canada, 14–23 June 2021; pp. 1–6.
23. Xu, J.; Ai, B. When mmWave high-speed railway networks meet reconfigurable intelligent surface: A deep reinforcement learning method. *IEEE Wirel. Commun. Lett.* **2021**, *11*, 533–537. [CrossRef]
24. Xu, J.; Ai, B.; Quek, T.Q. Towards Interference Suppression: RIS-Aided High-Speed Railway Networks via Deep Reinforcement Learning. *IEEE Trans. Wirel. Commun.* **2022**, *22*, 4188–4201. [CrossRef]
25. Ma, Z.; Wu, Y.; Xiao, M.; Liu, G.; Zhang, Z. Interference suppression for railway wireless communication systems: A reconfigurable intelligent surface approach. *IEEE Trans. Veh. Technol.* **2021**, *70*, 11593–11603. [CrossRef]
26. Chen, C.; Niu, Y.; Ai, B.; He, R.; Han, Z.; Zhong, Z.; Wang, N.; Su, X. Joint Design of Phase Shift and Transceiver Beamforming for Intelligent Reflecting Surface Assisted Millimeter-Wave High-Speed Railway Communications. *IEEE Trans. Veh. Technol.* **2022**, *72*, 6253–6267. [CrossRef]
27. Ai, B.; Molisch, A.F.; Rupp, M.; Zhong, Z.-D. 5G key technologies for smart railways. *Proc. IEEE* **2020**, *108*, 856–893. [CrossRef]
28. Wu, Q.; Zhang, R. Intelligent reflecting surface enhanced wireless network via joint active and passive beamforming. *IEEE Trans. Wirel. Commun.* **2019**, *18*, 5394–5409. [CrossRef]
29. Guo, W.; Zhang, W.; Mu, P.; Gao, F.; Lin, H. High-mobility wideband massive MIMO communications: Doppler compensation, analysis and scaling laws. *IEEE Trans. Wirel. Commun.* **2019**, *18*, 3177–3191. [CrossRef]
30. Gao, M.; Ai, B.; Niu, Y.; Wu, W.; Yang, P.; Lyu, F.; Shen, X. Efficient hybrid beamforming with anti-blockage design for high-speed railway communications. *IEEE Trans. Veh. Technol.* **2020**, *69*, 9643–9655. [CrossRef]
31. Ying, D.; Vook, F.W.; Thomas, T.A.; Love, D.J.; Ghosh, A. Kronecker product correlation model and limited feedback codebook design in a 3D channel model. In Proceedings of the 2014 IEEE International Conference on Communications (ICC), Sydney, Australia, 10–14 June 2014; pp. 5865–5870.
32. Wang, Q.; Zhou, F.; Hu, R.Q.; Qian, Y. Energy efficient robust beamforming and cooperative jamming design for IRS-assisted MISO networks. *IEEE Trans. Wirel. Commun.* **2020**, *20*, 2592–2607. [CrossRef]
33. Halder, S.; Sharma, H.K.; Biswas, A.; Prentkovskis, O.; Majumder, S.; Skačkauskas, P. On Enhanced Intelligent Water Drops Algorithm for Travelling Salesman Problem under Uncertain Paradigm. *Transp. Telecommun. J.* **2023**, *24*, 228–255. [CrossRef]
34. Grant, M.; Boyd, S.; Ye, Y. *CVX: Matlab Software for Disciplined Convex Programming*, version 2.0 beta; CVX Research: Austin, TX, USA, 2013.
35. Zhang, M.; Cumanan, K.; Thiyagalingam, J.; Wang, W.; Burr, A.G.; Ding, Z.; Dobre, O.A. Energy efficiency optimization for secure transmission in MISO cognitive radio network with energy harvesting. *IEEE Access* **2019**, *7*, 126234–126252. [CrossRef]
36. Boumal, N.; Mishra, B.; Absil, P.-A.; Sepulchre, R. Manopt, a Matlab toolbox for optimization on manifolds. *J. Mach. Learn. Res.* **2014**, *15*, 1455–1459.
37. Liu, Q.; Yang, J.; Xu, Y.; Li, G.; Sun, H. Energy-efficient resource allocation for secure IRS networks with an active eavesdropper. In Proceedings of the 2020 IEEE/CIC International Conference on Communications in China (ICCC), Chongqing, China, 9–11 August 2020; pp. 1–5.
38. Zhou, G.; Pan, C.; Ren, H.; Wang, K.; Peng, Z. Secure wireless communication in RIS-aided MISO system with hardware impairments. *IEEE Wirel. Commun. Lett.* **2021**, *10*, 1309–1313. [CrossRef]

39. Guo, H.; Liang, Y.-C.; Chen, J.; Larsson, E.G. Weighted sum-rate maximization for reconfigurable intelligent surface aided wireless networks. *IEEE Trans. Wirel. Commun.* **2020**, *19*, 3064–3076. [CrossRef]
40. Wang, T. Research on Wireless Resource Allocation Algorithm in High-Speed Rail Scenarios Based on Reinforcement Learning. Master's Thesis, Beijing Jiaotong University, Beijing, China, 2020.

Disclaimer/Publisher's Note: The statements, opinions and data contained in all publications are solely those of the individual author(s) and contributor(s) and not of MDPI and/or the editor(s). MDPI and/or the editor(s) disclaim responsibility for any injury to people or property resulting from any ideas, methods, instructions or products referred to in the content.